Energy Transport by Radiation in Hyperbolic Material Comparable to Conduction

Hakan Salihoglu, Vasudevan Iyer, Takashi Taniguchi, Kenji Watanabe, Peide D. Ye, and Xianfan Xu*

Radiation as a heat transfer mode inside a bulk material is usually negligible in comparison to conduction. Here, the contribution of radiation to energy transport inside a hyperbolic material, hexagonal boron nitride (hBN), is investigated. With hyperbolic dispersion, i.e., opposite signs of dielectric components along principal directions, phonon polaritons contribute significantly to energy transport due to a much greater number of propagating modes compared to that in a normal material. A many-body model is developed to account for radiative heat transfer in a material with a nonuniform temperature distribution. The total radiative heat transfer through hBN is found to be largely contributed by the high-κ modes within the Reststrahlen bands, and is comparable to phonon conduction. Experimental measurements of temperature-dependent thermal transport also show that radiative contribution to thermal transport is of the same order as that from phonons. Therefore, this work shows, for the first time, radiative heat transfer inside a material can be comparable to phonon conductive heat transfer.

1. Introduction

In solids, it has been understood that the primary energy carriers are phonons and electrons. Another energy carrier, photons, has been treated as a surface phenomenon, and as such, its contribution to energy transfer inside a material is negligible. However, the role of photons in thermal transport is also originated from the bulk. Rytov's seminal work employed the fluctuation dissipation theorem (FDT) to link thermal fluctuations in a material with the generated electromagnetic energy, which enabled prediction of radiative emission from

H. Salihoglu, V. Iyer, Prof. X. Xu
School of Mechanical Engineering and Birck Nanotechnology Center
Purdue University
West Lafayette, IN 47907, USA
E-mail: xxu@ecn.purdue.edu
Dr. T. Taniguchi, Dr. K. Watanabe
National Institute for Materials Science
Namiki 1-1, Tsukuba, Ibaraki 305-0044, Japan
Prof. P. D. Ye
School of Electrical and Computer Engineering and Birck
Nanotechnology Center
Purdue University
West Lafayette, IN 47907, USA

The ORCID identification number(s) for the author(s) of this article can be found under https://doi.org/10.1002/adfm.201905830.

the material in equilibrium.[1] Recently, the extent of FDT was expanded for near-field radiation arising from evanescent waves or resonant surface waves.[2–8] The large enhancement of near-field thermal radiation has brought about a myriad of potential applications such as near-field thermophotovoltaics,[9] thermal diode,[10] and thermal infrared near-field spectroscopy.[11,12] The much enhanced thermal radiation in extreme near-field implies strong electromagnetic interactions in the bulk, and is predicted by FDT well.[13]

Radiative waves inside a conductor induced by thermal fluctuations vanish over a short length on the order of 10 nm. Wave propagation supported in dielectric materials is limited to wave vectors confined in the light cone. Hyperbolic materials (HMs), on the other hand, allow long wave propagation with large wave vectors. The permittivity of HM exhibits anisotropic behaviors with opposite signs for the in-plane (x,y) and out-of-plane (z) components ($\varepsilon_{x,y} > 0$ and $\varepsilon_z < 0$ for Type I, and vice versa for Type II) in the Reststrahlen bands. This leads to a hyperboloidal κ-space contour and hence propagating hyperbolic waves or phonon-polaritons with wave vectors much larger than the light cone in the HM material.[14,15] HMs have already shown promises in near-field radiation, including optical imaging,[16] long range Coulombic interactions inside a material,[17] thermal emission engineering,[18,19] and conical nanoresonators supporting sub-diffractional volume-confined polaritons in the material.[20]

The range of allowed propagating phonon-polariton modes in HM depends on its building blocks. HM[21] can be made of layered structures or nanowires in a host medium. The periodicity of building blocks, the thickness of the layers or the separation distance of the nanowires, constrains the maximum wave vector supported in the medium. On the other hand, natural HMs[22] comprise periodic array of atoms. In theory, waves with wave vector up to $\approx \pi/a$, where a is the lattice constant, are supported. There are a number of experimental studies[20,23–26] on phonon-polaritons in HMs. Phonon-polariton modes with $\kappa \sim \pi/a$ are expected to be confined in the bulk[12] and have yet to be observed.

hBN is an extensively studied natural HM due to its low loss. Coupled phonon-polaritons in mid-IR in hBN nanodisks have been predicted to enhance the Purcell factor, also referred to as the density of photonic states,[27] by a factor of 80 000 in

ADVANCED
SCIENCE NEWS
www.advancedsciencenews.com

ADVANCED
FUNCTIONAL
MATERIALS
www.afm-journal.de

the region between the disks.[28] Propagating high-κ phonon-polaritons in hBN also enables imaging structures and defects with a resolution beyond the diffraction limit.[29] From the heat transfer perspective, the dominant in-plane phonon interactions yield high bulk thermal conductivity, $\approx$400 W m^{-1} K^{-1} at room temperature,[30] which decreases with the well-known $1/T$ trend[31] due to the intrinsic Umklapp scattering.[32] Weak phonon interactions from van der Waals forces in the out-of-plane direction result in a thermal conductivity of about 5 W m^{-1} K^{-1} in bulk hBN.[33] Along the out-of-plane direction, propagation of phonon-polaritons with high-κ modes can contribute to appreciable thermal transport. For example, the coupled electron-polariton modes in hBN/graphene stack resulted in enhanced heat transfer by super-Planckian emission.[34] Furthermore, owing to electromagnetic nature of the coupling, these modes transport energy across hBN/graphene interface faster than phonon coupling.[35] However, direct study of the hyperbolic phonon-polariton contribution to radiative transfer (hyperbolic blackbody radiation) inside hBN or HM has not been reported.

In this work, contribution of hyperbolic high-κ modes to radiative heat transfer (hyperbolic blackbody radiation) in hBN in the out-of-plane direction is investigated. While most recent researches on near-field thermal radiation focus on energy transport across nanometric gaps, this work instead investigates the role of thermal radiation inside the material. A method to analyze spectral and total radiative heat transfer through HM as a function of temperature and thickness of the material is developed. This method computes "radiative thermal conductivity" originated from the propagating waves in the material. Results show that the thermally excited high-κ modes can be a contributing energy transport channel. The results also predict that the radiative contribution increases with the temperature rise, and has the same order of magnitude compared with the phonon contribution. Experimental measurements of the total heat transfer agree with theoretical predictions.

2. Results and Discussion

Our microscopic many-body model consists of a continuous medium, under investigation, sandwiched by two heat baths (**Figure 1**A). The medium is divided into many bodies (slabs) in the z-direction (out-of-plane, $\perp$) and extends to infinity in x- and y-directions. Each slab is assumed to be in local thermal
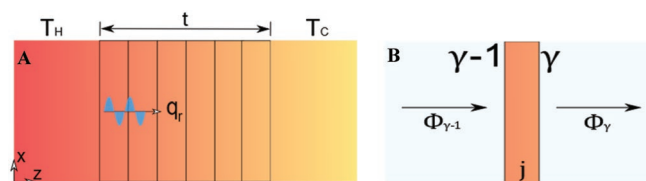

Figure 1. Microscale many-body model. A) Schematic of the radiative heat transfer problem under investigation. Combination of slabs forms a continuous medium. The medium is in contact with two heat baths of prescribed temperatures, T_H and T_C. B) Control volume around a single slab and energy transfer. $\Phi_{\gamma-1}$ and Φ_γ are evaluated at interfaces $\gamma - 1$ and γ, respectively. $\Phi_{\gamma-1} = \Phi_\gamma$ represents local thermal equilibrium condition for the single slab.

equilibrium at a local temperature, hence radiative thermal energy flux, S ($E \times H$), from the slab is calculated by means of FDT. The energy flux is continuous in the out-of-plane direction owing to the continuity of tangential components of E and H throughout the system. Considering contribution of all slabs at interfaces allows computing radiative heat flux arising from electromagnetic interactions through a continuous material out of thermal equilibrium. Specifically, the heat flux (Φ) into a slab (j) across an interface (γ) is a result of superposed electromagnetic waves from all thermal sources interacting with media along the path from the source. The net heat flux into slab j can be expressed in a Landauer-like form as (Figure 1B, details are given in Section S1, Supporting Information)[36]

$$\Phi^j = \Phi_{\gamma-1} - \Phi_\gamma = \int_0^\infty \frac{d\omega}{2\pi} \int_0^{\kappa_{max}} \frac{d\kappa}{2\pi} \kappa \sum_{s,p} \sum_{l=0}^N \Theta_{l,j} \mathcal{T}^{l,j} \quad (1)$$

where ω, κ, s, and p are frequency, wavenumber, and transverse-electric and transverse-magnetic polarizations, respectively. $\Theta_{l,j}$ represents the difference in mean energy of oscillators generated in slabs l and j. The energy exchange function, $\mathcal{T}^{l,j}$, accounts for energy exchange between slabs l and j, and is expressed as $(1 - |\tau_l|^2)|\tau^{l+1 \to j-1}|^2(1 - |\tau_j|^2)$. The transmission coefficient, τ, derived using the scattering matrix method (see Section S1, Supporting Information), represents energy transmitted through a single slab j, $\tau_j = e^{i\kappa_{\perp,j}\delta_j}$, as well as all the slabs from $l + 1$ to $j - 1$, $\tau^{l+1 \to j-1} = e^{i\sum_{m=l+1}^{j-1} \kappa_{\perp,m}\delta_m}$, where $\kappa_{\perp,m}$ and δ_m are out-of-plane component of wavevector through slab m and the thickness of the slab, respectively. Details regarding derivations of $\mathcal{T}$ and τ are given in Section S1 in the Supporting Information. The summation over l in Equation (1) implies that slab j interacts with all other slabs. Regarding the limits of integration in Equation (1), $\kappa_{max} = \sqrt{\varepsilon}\,\omega/c$ outside the Reststrahlen bands, and extends to $\approx \pi/a$ in the Reststrahlen bands. It is known that the maximum wavevector is influenced by multiple factors.[37] In this work, atomic lattice constants are used to calculate the cut-off, which are 0.24 and 0.66 nm for in- and out-of-plane directions, respectively.[38]

Equation (1) is solved to obtain an energy balance condition for each slab: $\Phi_{\gamma-1} = \Phi_\gamma$. Hence, the total radiative heat transfer is simply Φ_γ. An initial temperature distribution is first assumed, and Φ^j are computed. Calculations are iterated until $\Phi_{\gamma-1} = \Phi_\gamma$ is satisfied for each slab and then a temperature distribution is also obtained. We validated the method for two blackbodies separated by far-field distances emitting at prescribed temperatures (Figure S1, Supporting Information). It is also shown that Equation (1) is a general expression for hyperbolic blackbodies (Section S2, Supporting Information).

We first look at the transmission coefficient τ. **Figure 2**A–C illustrates the transmission coefficients with respect to frequency and wave vector for p-polarized waves (phonon-polaritons) over a thickness of $d = 10$ nm, 100 nm, and 10 µm, respectively. The majority of phonon-polaritons with very high wave vectors (here defined as $\kappa > 10^8$ m^{-1}, thus $\lambda < 10$ nm) carry energy over a distance of about 10 nm without significant loss (Figure 2A); however, these carriers lose over 80% of their energies over a distance of 100 nm because of the exponential decay $e^{-2\kappa''d}$ (Figure 2B). For phonon-polaritons with wave vectors in the range $10^7 < \kappa < \approx 10^8$ m^{-1} (defined as high-κ
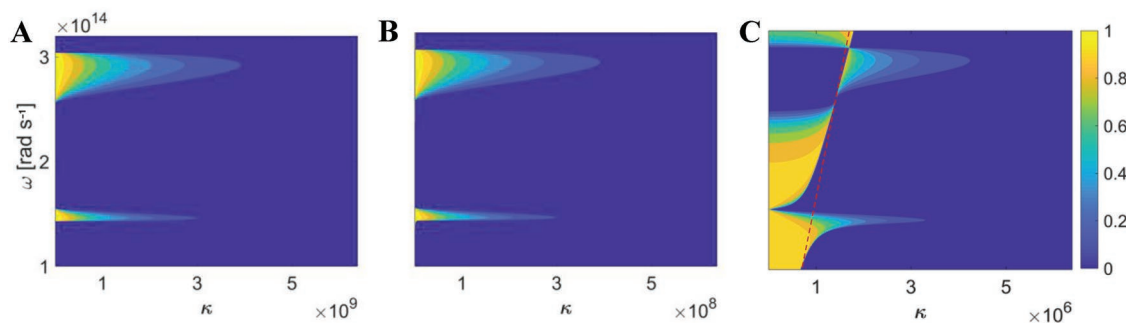
Figure 2. Transmission coefficients of p-polarized waves over a thickness of A) 10 nm, B) 100 nm, and C) 10 μm. Scales and ranges of the γ-axis for (A) to (C) are the same. Both high-κ ($10^7 < \kappa < 10^8$ m^{-1}) and very high-κ ($\kappa \sim \pi/a > 10^8$ m^{-1}) modes transfer energy in 10 nm, whereas very high-κ modes mostly attenuate over a thickness of about 100 nm. Red dashed line in (C) corresponds to the modes with $\kappa \sim n\omega/c$.

phonon-polaritons here, corresponding to $100 > \lambda > 10$ nm), a distance greater than 1 μm nulls their contribution (Figure 2B). For phonon-polaritons with even smaller κ values ($\kappa \sim 10^6$ m^{-1}, thus $\lambda \sim 1$ μm), its decay distance is about of 10 μm (Figure 2C).

We next examine spectral radiative heat transfer across the medium at room temperature (300 K). A 1 K temperature difference between the heat baths is imposed to drive radiative heat transfer in hBN. **Figure 3**A shows the spectral radiative heat transfer which has two characteristic peaks in the Reststrahlen bands, arising from the available large number of modes and resulting in super-Planckian emission. Phonon-polaritons transport energy via all transport channels (modes) at frequencies inside the Reststrahlen bands, producing six orders of magnitude higher radiative transport compared to that outside the Reststrahlen bands. The reason that the spectral radiation outside the Reststrahlen bands exceeds that of blackbody in vacuum (Figure 3A) is due to the higher index of refraction of hBN than vacuum ($n > 1$).

We further analyze contributions of all modes over the entire frequency range, i.e., the total radiative heat transfer. The total radiative heat transfer depends on material's thickness, as suggested by the previous analysis on the dependence of transmission coefficient of phonon-polariton modes on thickness. Figure 3B shows that the total radiative heat transfer decreases with thickness. Here, the density of modes as a function of

wave vector plays the key role. The greatest contribution to total radiative heat transfer in short distances comes from very high-κ phonon-polaritons as the high density of energy channels (modes) for very high-κ phonon-polaritons enables energy transport with a large number of energy carriers. However, the energy carried by these modes dissipates rapidly over short distances as seen in the spectral analysis. As the distance increases, less carriers contribute to transferring energy, leading to a decrease in total heat transfer.

We can also compute an equivalent conductivity caused by radiative heat transfer, $k_{rad} = q_r'' t/\Delta T$ solely for the purpose of comparing with conduction heat transfer. Here, q_r'' is the total radiative heat transfer, t is the thickness, and ΔT is the temperature difference of the two heat baths. Figure 3B shows that k_{rad} increases with t and approaches a constant value at ≈500 nm. In thin hBN, k_{rad} increases with thickness since the number of energy carrier that vanishes due to dissipation is less than that excited by adding more material to the medium. The conductivity reaches a constant value at the thickness ≈500 nm as the number of disappeared carriers and that of the added carriers reach a balance.

We now investigate radiative heat transfer at elevated temperatures. The dielectric properties of the material that govern propagation/dissipation of phonon-polaritons are temperature dependent. **Figure 4**A,B shows dielectric properties of hBN from 300 to 600 K, extracted from FTIR (Fourier transform
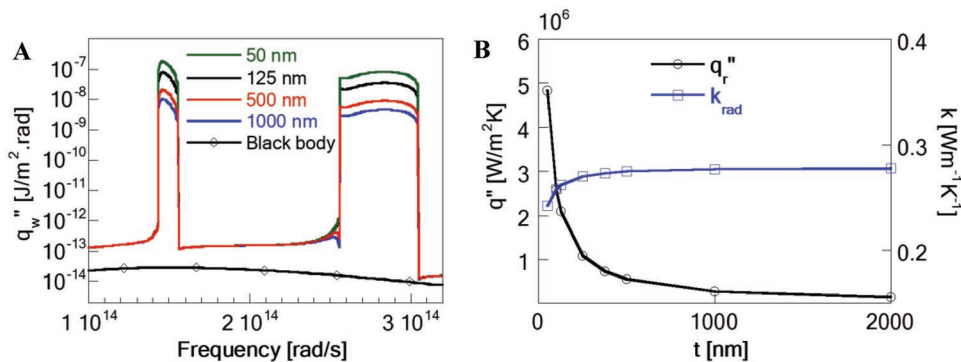

Figure 3. Spectral and total radiative heat transfer with respect to thickness. A) Spectral radiation transfer in hBN with 1 K temperature difference between heat baths. The enhancement within the Reststrahlen bands clearly demonstrates contributions of phonon polariton modes. B) Total radiation and radiative thermal conductivity at various thicknesses. The contribution of very high-κ modes to radiative transport decreases with thickness due to losses in thicker films.
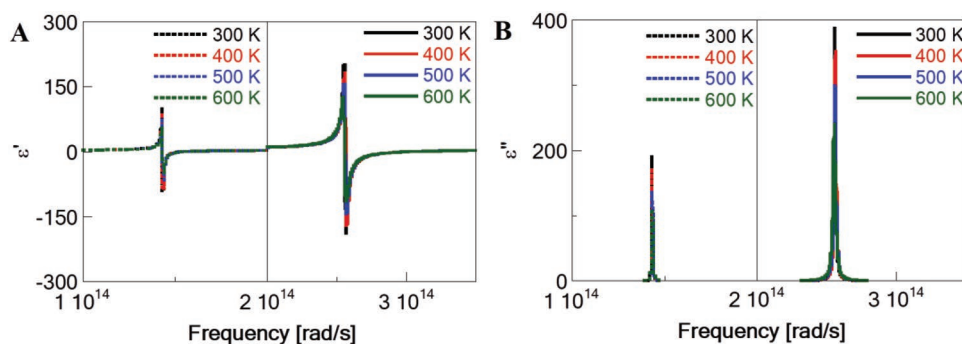
Figure 4. Temperature-dependent dielectric properties. A,B) Real and imaginary components of dielectric permittivity over the Reststrahlen bands at various temperatures. The dashed lines with frequency less than 2×10^{14} rad s^{-1} are out-of-plane component (Type I), and the solid lines with frequency greater than 2×10^{14} rad s^{-1} are in-plane component (Type II).

infrared spectroscopy) measurements (see the Experimental Section, Section S3 and Figure S2, Supporting Information). Despite the temperature dependency of dielectric properties, phonon-polaritons at elevated temperatures transport energy approximately over the similar distance as those at room temperature (see Section S4 and Figure S3, Supporting Information).

We calculated the temperature-dependent radiative thermal conductivity by raising the temperatures of the thermal baths, but maintained the temperature difference at 1 K. **Figure 5**A shows radiative thermal conductivity increases with temperature. Raising the temperature excites a larger number of energy states and also shifts thermal energy peak towards higher frequencies according to the Wien's displacement law, which will be further discussed. We notice that the measured thermal conductivity at 300 K is in good agreement with the literature data.[33] At this temperature, the radiative contribution is relatively small.

We measure the out-of-plane (in the direction perpendicular to the thin film) total thermal conductivity in hBN thin films using a time-domain thermal reflectance method (see the Experimental Section and Section S5, Supporting Information),[39] in the temperature range from 300 to 600 K. The measured thermal conductivity, $k_{Tot,exp}$, contains both photonic (phonon polariton modes) and phononic contributions, and is

shown in Figure 5A for a 1030 nm thick hBN film. The validity of extracting a total thermal conductivity was examined by computing conduction heat transfer and radiative transfer separately using the temperature history at each time step, and comparing with the result computed using a total thermal conductivity. It was found that two results are identical, which is due to the low temperature rise (a few degrees) in the experiments and hence linearizing phonon-polariton contribution is a good approximation. We can see that there is a decrease of the measured total thermal conductivity from 300 to 600 K. However, this decrease is much slower than the $1/T$ dependence for phonon transport alone, which suggests a temperature-dependent phonon-polariton radiative contribution. We calculate the difference between the calculated radiation thermal conductivity k_{rad} and the experimentally determined $k_{Tot,exp}$, which yields the experimental phonon conductivity, $k_{Phonon,exp}$, as shown in Figure 5B. The resulting $k_{Phonon,exp}$ follows a much closer $1/T$ trend of phonon conductivity, which will be further discussed below.

We notice a large contribution of radiative thermal transport as the temperature increases, from ≈5% at 300 K to ≈27% at 600 K. The increase of radiative thermal conductivity with temperature originates from the increased contribution of thermally excited phonon-polaritons in the Reststrahlen band. The peak radiation at 300 K is at a frequency around ≈10 μm (≈1.9×10^{14} rad s^{-1}), which is below the lower bound of the
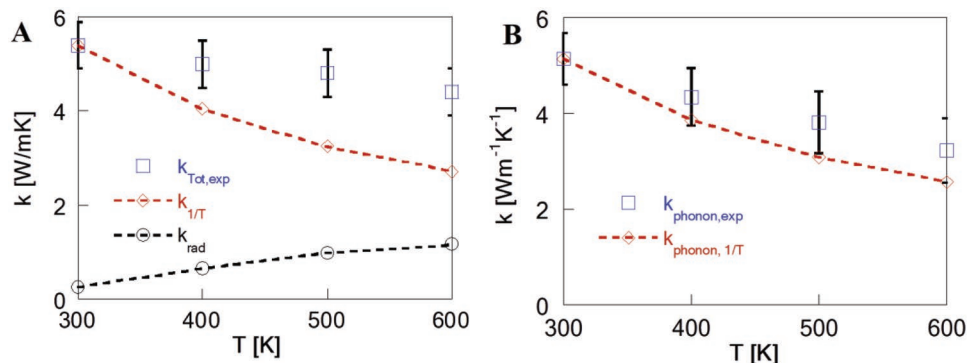

Figure 5. Radiative thermal conductivity. A) Radiative thermal conductivity k_{rad} and measured total thermal conductivity ($k_{Tot,exp}$) with respect to temperature. The total thermal conductivity consists of both photonic and phononic contributions, and does not follow the normal $1/T$ dependence of phonon conductivity (red dashed line). B) Experimental phonon thermal conductivity $k_{Phonon,exp}$ obtained by subtracting k_{rad} from $k_{Tot,exp}$ and comparison to the $1/T$ dependence of phonon conductivity.

Reststrahlen band (2.5×10^{14} rad s^{-1}). Increasing temperature increases populated photon states with thermal energy inside the Reststrahlen band. At 400 K, the peak radiation moves into the Reststrahlen band, and at higher temperatures, it moves toward the upper bound of the Reststrahlen band (3×10^{14} rad s^{-1}). Moreover, the radiative thermal conductivity increases due to higher energy carried by the phonon-polariton at higher temperature.

We now discuss the small deviation of the extracted $k_{Phonon,exp}$ versus the expected $1/T$ phonon conductivity. This can be a result of experimental uncertainties, as indicated in the error bars of the measured total thermal conductivity which is about $+/-0.5$ W m^{-1} K^{-1} (details in Section S5, Supporting Information). Computation of radiative thermal conductivity uses dielectric constants, which were also measured experimentally using FTIR (Section S3, Supporting Information). We estimate that the uncertainty in dielectric constant measurement can contribute up to 20% of uncertainty in the calculated radiative thermal conductivity (Section S3, Supporting Information). Given these considerations, the extracted $k_{Phonon,exp}$ is in a reasonable agreement with the expected $1/T$ trend. On the other hand, we also notice a recent study on the out-of-plane thermal conductivity of hBN which showed that thermal conductivity does not follow $1/T$ in a temperature range between over 100 and 400 K.[33] This deviation was attributed to the contribution of high-frequency acoustic phonons which do not follow the $1/T$ trend at temperatures below 400 K. At temperatures above 400 K, however, the contribution of high-frequency phonons also decreases with temperature, resulting in $\approx 1/T$ trend in phonon thermal conductivity.

Lastly, we emphasize the contribution of high-κ phonon-polariton modes to radiative thermal transport. Phonon polaritons and phonons in HM coexist and both contribute to energy transport. In a normal material, the spherical or ellipsoidal κ-space contour limits the wave vector, and the modes with wave vectors greater than that of the light cone do not propagate, i.e., resulting in Planckian emission. On the other hand, in the Reststrahlen bands of HMs, the hyperboloidal κ-space which is a result of opposite signs of the dielectric constants along the principal directions, allows propagations of phonon-polaritons with wave vectors larger than the light cone, resulting in super-Planckian emission. The number of modes with wave vectors larger than the light cone is very large in the Reststrahlen bands. Various studies[40–42] also suggested that the maximum wave vector should be cut off at $\kappa \sim \pi/a$. Hence, high-κ phonon-polariton modes in bulk are responsible for the rise of the notable radiative contribution. We note that the use of a large wavevector cut off results in a high refractive index of $\approx 10^4$ in the Reststrahlen bands ($\kappa_{max} = \pi/a = n\omega/c$), where as in literature a nanoresonator 86 times smaller than free space wavelength was observed.[20]

3. Conclusion

In summary, we studied radiative heat transfer in HM hBN and showed a major contribution to energy transport arising from phonon polaritons supported in the Reststrahlen bands. This contribution increases spectral radiative transfer by six orders of magnitude inside the Reststrahlen bands compared to that outside the Reststrahlen bands. The equivalent radiative thermal conductivity increases with temperature increase, and the radiative thermal conductivity can be of the same order of the phonon thermal conductivity. Experimental measurements support our finding. The measured temperature-dependent total thermal conductivity does not follow the usual $1/T$ phonon conductivity, which is attributed to the increase in radiative thermal conductivity with temperature. We showed the radiative contribution can account for as much as 27% of the total thermal transport at 600 K. Hence, in hBN the radiative thermal transport can be comparable to thermal conduction by phonons.

4. Experimental Section

Sample Preparation: Ultrapure hBN films were exfoliated a few times with Nitto dicing tape and subsequently transferred onto a thermal release tape (Nitto), which was adhered to the silicon substrate. The tape was release by heating the substrate to 120 °C to obtain clean and high yield transfer of hBN films with various thicknesses. Within a few hours of exfoliation, 110 nm gold was deposited on the entire sample using e-beam evaporation for thermal conductivity measurement. The sample was cleaned with toluene, acetone, and isopropyl alcohol just before the gold deposition. Atomic force microscopy (AIST-NT) scans were performed after gold deposition to precisely determine the film thicknesses.

Temperature-Dependent Dielectric Properties: Nexus 670 FTIR Bench with a Continuum Microscope to collect reflection spectra of ≈ 1 μm thick hBN on bulk CaF$_2$ was used. Sample was placed on a Linkam THMS720 heating stage to control its temperature. After temperature stabilization, reflected light collected by a 15x objective lens was averaged over 64 scans. Measurement was repeated to ensure the repeatability of data. The Lorentz model with one oscillator for both components of dielectric permittivity agreed with the temperature-dependent reflection data. Details are shown in Section S3 in the Supporting Information.

Thermal Conductivity Measurement: Thermal conductivity was measured with a home-built nanosecond thermoreflectance setup.[39] The sample was pumped to higher temperature ($T_{excess} < 7$ K) with a 6.4 ns, 5 kHz pulsed laser (Spectra Physics) operating at 532 nm wavelength. The change in surface temperature was measured with a continuous wave He-Ne probe laser beam coupled to a balanced fast photodiode (Thorlabs PDB130A), and directly recorded on a high speed oscilloscope (Tektronix TDS744A) set to AC coupling mode averaging 10 000 acquisitions. The pump beam was expanded to a 164 μm $1/e^2$ diameter to minimize in-plane heat diffusion. The probe spot was 20 μm in diameter. The sample was mounted on a heating stage (Linkam THMS 720) and annealed at 600 K for 1 h before performing temperature-dependent measurements. The measurements were repeated several times to ensure reproducibility. The acquired data was fit with COMSOL using a transient 2D axisymmetric model to extract the thermal conductivity (see Section S5, Supporting Information).

Supporting Information

Supporting Information is available from the Wiley Online Library or from the author.

Acknowledgements

ADVANCED
SCIENCE NEWS

www.advancedsciencenews.com

ADVANCED
FUNCTIONAL
MATERIALS

www.afm-journal.de

Conflict of Interest

The authors declare no conflict of interest.

Keywords

[1] S. M. Rytov, *Theory of Electric Fluctuations and Thermal Radiation*, Force Cambridge Research Center, Bedford, MA **1959**.

[2] D. Polder, M. Van Hove, *Phys. Rev. B* **1971**, *4*, 3303.

[3] J. J. Loomis, H. J. Maris, *Phys. Rev. B* **1994**, *50*, 18517.

[4] K. Joulain, J.-P. Mulet, F. Marquier, R. Carminati, J.-J. Greffet, *Surf. Sci. Rep.* **2005**, *57*, 59.

[5] M. Francoeur, M. P. Mengüç, R. Vaillon, *Appl. Phys. Lett.* **2008**, *93*, 043109.

[6] S. Shen, A. Narayanaswamy, G. Chen, *Nano Lett.* **2009**, *9*, 2909.

[7] R. St-Gelais, B. Guha, L. Zhu, S. Fan, M. Lipson, *Nano Lett.* **2014**, *14*, 6971.

[8] A. Fiorino, D. Thompson, L. Zhu, B. Song, P. Reddy, E. Meyhofer, *Nano Lett.* **2018**, *18*, 3711.

[9] A. Fiorino, L. Zhu, D. Thompson, R. Mittapally, P. Reddy, E. Meyhofer, *Nat. Nanotechnol.* **2018**, *13*, 806.

[10] A. Fiorino, D. Thompson, L. Zhu, R. Mittapally, S.-A. Biehs, O. Bezencenet, N. El-Bondry, S. Bansropun, P. Ben-Abdallah, E. Meyhofer, P. Reddy, *ACS Nano* **2018**, *12*, 5774.

[11] A. C. Jones, M. B. Raschke, *Nano Lett.* **2012**, *12*, 1475.

[12] Z. Shi, H. A. Bechtel, S. Berweger, Y. Sun, B. Zeng, C. Jin, H. Chang, M. C. Martin, M. B. Raschke, F. Wang, *ACS Photonics* **2015**, *2*, 790.

[13] L. Cui, W. Jeong, V. Fernández-Hurtado, J. Feist, F. J. García-Vidal, J. C. Cuevas, E. Meyhofer, P. Reddy, *Nat. Commun.* **2017**, *8*, 14479.

[14] P. Shekhar, J. Atkinson, Z. Jacob, *Nano Convergence* **2014**, *1*, 14.

[15] W. Ma, P. Alonso-González, S. Li, A. Y. Nikitin, J. Yuan, J. Martín-Sánchez, J. Taboada-Gutiérrez, I. Amenabar, P. Li, S. Vélez, C. Tollan, Z. Dai, Y. Zhang, S. Sriram, K. Kalantar-Zadeh, S.-T. Lee, R. Hillenbrand, Q. Bao, *Nature* **2018**, *562*, 557.

[16] P. Li, M. Lewin, A. V. Kretinin, J. D. Caldwell, K. S. Novoselov, T. Taniguchi, K. Watanabe, F. Gaussmann, T. Taubner, *Nat. Commun.* **2015**, *6*, 7507.

[17] W. D. Newman, C. L. Cortes, A. Afshar, K. Cadien, A. Meldrum, R. Fedosejevs, Z. Jacob, *Sci. Adv.* **2018**, *4*, eaar5278.

[18] Y. Guo, Z. Jacob, *Opt. Express* **2013**, *21*, 15014.

[19] H. Salihoglu, X. Xu, *J. Quant. Spectrosc. Radiat. Transfer* **2019**, *222–223*, 115.

[20] J. D. Caldwell, A. V. Kretinin, Y. Chen, V. Giannini, M. M. Fogler, Y. Francescato, C. T. Ellis, J. G. Tischler, C. R. Woods, A. J. Giles, M. Hong, K. Watanabe, T. Taniguchi, S. A. Maier, K. S. Novoselov, *Nat. Commun.* **2014**, *5*, 5221.

[21] J. Shi, B. Liu, P. Li, L. Y. Ng, S. Shen, *Nano Lett.* **2015**, *15*, 1217.

[22] E. E. Narimanov, A. V. Kildishev, *Nat. Photonics* **2015**, *9*, 214.

[23] S. Dai, Q. Ma, T. Andersen, A. S. Mcleod, Z. Fei, M. K. Liu, M. Wagner, K. Watanabe, T. Taniguchi, M. Thiemens, F. Keilmann, P. Jarillo-Herrero, M. M. Fogler, D. N. Basov, *Nat. Commun.* **2015**, *6*, 6963.

[24] D. Hu, X. Yang, C. Li, R. Liu, Z. Yao, H. Hu, S. N. G. Corder, J. Chen, Z. Sun, M. Liu, Q. Dai, *Nat. Commun.* **2017**, *8*, 1471.

[25] L. V. Brown, M. Davanco, Z. Sun, A. Kretinin, Y. Chen, J. R. Matson, I. Vurgaftman, N. Sharac, A. J. Giles, M. M. Fogler, T. Taniguchi, K. Watanabe, K. S. Novoselov, S. A. Maier, A. Centrone, J. D. Caldwell, M. Nanocenter, *Nano Lett.* **2018**, *18*, 1628.

[26] Z. Zheng, J. Chen, Y. Wang, X. Wang, X. Chen, P. Liu, J. Xu, W. Xie, H. Chen, S. Deng, N. Xu, Z. Zheng, X. Wang, H. Chen, S. Deng, N. Xu, J. Chen, Y. Wang, X. Chen, P. Liu, W. Xie, J. Xu, *Adv. Mater.* **2018**, *30*, 1705318.

[27] A. P. Slobozhanyuk, P. Ginzburg, D. A. Powell, I. Iorsh, A. S. Shalin, P. Segovia, A. V. Krasavin, G. A. Wurtz, V. A. Podolskiy, P. A. Belov, A. V. Zayats, *Phys. Rev. B* **2015**, *92*, 195127.

[28] M. Tamagnone, A. Ambrosio, K. Chaudhary, L. A. Jauregui, P. Kim, W. L. Wilson, F. Capasso, *Sci. Adv.* **2018**, *4*, eaat7189.

[29] S. Dai, M. Tymchenko, Z.-Q. Xu, T. T. Tran, Y. Yang, Q. Ma, K. Watanabe, T. Taniguchi, P. Jarillo-Herrero, I. Aharonovich, D. N. Basov, T. H. Tao, A. Alù, *Nano Lett.* **2018**, *18*, 5205.

[30] I. Jo, M. T. Pettes, J. Kim, K. Watanabe, T. Taniguchi, Z. Yao, L. Shi, *Nano Lett.* **2013**, *13*, 550.

[31] G. Qin, Z. Qin, H. Wang, M. Hu, *Phys. Rev. B* **2017**, *95*, 195416.

[32] S. Mukhopadhyay, D. S. Parker, B. C. Sales, A. A. Puretzky, M. A. Mcguire, L. Lindsay, *Science* **2018**, *360*, 1455.

[33] P. Jiang, X. Qian, R. Yang, L. Lindsay, *Phys. Rev. Mater.* **2018**, *2*, 64005.

[34] K.-J. Tielrooij, N. C. H. Hesp, A. Principi, M. B. Lundeberg, E. A. A. Pogna, A. Banszerus, Z. Mics, M. Massicotte, P. Schmidt, D. Davydovskaya, D. G. Purdie, I. Goykhman, G. Soavi, A. Lombardo, K. Watanabe, T. Taniguchi, M. Bonn, D. Turchinovich, C. Stampfer, A. C. Ferrari, G. Cerullo, M. Polini, F. H. L. Koppens, *Nat. Nanotechnol.* **2018**, *13*, 41.

[35] W. Yang, S. Berthou, X. Lu, Q. Wilmart, A. Denis, M. Rosticher, T. Taniguchi, K. Watanabe, G. Fève, J.-M. Berroir, G. Zhang, C. Voisin, E. Baudin, B. Plaçais, *Nat. Nanotechnol.* **2018**, *13*, 47.

[36] I. Latella, P. Ben-Abdallah, S.-A. Biehs, M. Antezza, R. Messina, *Phys. Rev. B* **2017**, *95*, 205404.

[37] S. Molesky, Z. Jacob, *Phys. Rev. A* **2019**, *99*, 33833.

[38] A. J. Giles, S. Dai, I. Vurgaftman, T. Hooman, S. Liu, L. Lindsay, C. T. Ellis, N. Assefa, I. Chatzakis, T. L. Reinecke, J. G. Tischler, M. M. Fogler, J. H. Edgar, D. N. Basov, J. D. Caldwell, *Nat. Mater.* **2018**, *17*, 134.

[39] R. Garrelts, A. Marconnet, X. Xu, *Nanoscale Microscale Thermophys. Eng.* **2015**, *19*, 245.

[40] T. G. Pedersen, *Phys. Rev. B* **2003**, *67*, 113106.

[41] A. I. Volokitin, B. N. J. Persson, *Phys. Rev. B* **2004**, *69*, 045417.

[42] A. N. Poddubny, P. A. Belov, P. Ginzburg, A. V. Zayats, Y. S. Kivshar, *Phys. Rev. B* **2012**, *86*, 035148.